Supporting Information for "A Linear Response Framework for Radiative-Convective Instability"

Tom Beucler[1],Timothy Cronin[1], Kerry Emanuel[1]

1. Introduction

The following section takes one step towards the real world by applying the linear response framework of section 2 to a full-physics column model. Because the column model is calibrated to work on climatological ($\sim$ 100day) rather than convective ($\sim$ 3hours) time scales, both the methodology and the results are complex. The reader may skip this section without missing fundamental aspects of radiative-convective instability.

Corresponding author: Tom Beucler, Lorenz Center, Department of Earth Atmospheric and Planetary Sciences, Massachusetts Institute of Technology, Cambridge, MA 02139, USA. (tom.beucler@gmail.com)

[1]Lorenz Center, Department of Earth
Atmospheric and Planetary Sciences,
Massachusetts Institute of Technology,
Cambridge, MA 02139, USA.

2. Experimental design

We choose to construct the linear response matrix of the MIT single-column model, first described in *Renno et al.* [1994], because its convection scheme (see *Emanuel and Živković-Rothman* [1999]; *Emanuel* [1991]) includes unsaturated downdrafts, which have not been explicitly parametrized in the previous sections, and it conserves column moist static energy. Its radiation scheme is based off the European Center for Medium Weather Forecasts forecasting system *Morcrette* [1991]; *Fouquart and Bonnel* [1980]. We run the model with a tropospheric resolution of 25hPa and 60 levels in total. It has fully interactive radiation, convection, and water vapor, called at every timestep. Although the model produces cloud, we deactivate cloud-radiation interactions to focus on the clear-sky response matrix. We also deactivate the convective gustiness, as well as its associated temperature and moisture Reynolds corrections. To avoid abrupt and nonlinear jumps in the deep convective profiles, we relax the level of neutral buoyancy in time, so that it linearly responds to convection with a one-hour lag:

$$\frac{\partial p_{\mathrm{NB}}}{\partial t} = \frac{p_{\mathrm{NB,Emanuel}} - p_{\mathrm{NB}}}{\tau_{\mathrm{NB}}}, \tag{1}$$

where $p_{\mathrm{NB,Emanuel}}$ is the level of neutral buoyancy computed by the Emanuel convective routine, p_{NB} is the "relaxed" level of neutral buoyancy and $\tau_{\mathrm{NB}} = 1$hours is the relaxation timescale. Our experiment consists of 5 steps:

1. We run the model to RCE. The initial conditions are climatological temperature and specific humidity profiles from the tropical Western-Pacific island of Chuuk-Lagoon (Micronesia), and we use a monthly-averaged ERA-Interim reanalysis *Dee et al.* [2011] ozone profile (spatially-averaged in the (2°,2°) box centered around Chuuk Lagoon, during

the month of January 2016). The only other greenhouse gas is carbon dioxide, assumed to be well-mixed, with a constant volume concentration of 400ppmv. We prescribe a fixed surface wind of 5ms^{-1} and a fixed sea surface temperature of 300K. Other relevant parameters for this run is described in Table 1. The temperature and specific humidity profiles adjust to a unique statistical equilibrium, independent of the initial climatological profile, and in which the time-averaged dry static energy and water vapor forcings are zero on timescales longer than a few days.

2. To capture the statistical nature of RCE, we select 100 snapshots of RCE and perturb each of their water vapor profiles level by level. For each water vapor profile, 38 "moistened" profiles are produced, by adding 1% to the specific humidity at each level, one at a time, between the top of the subcloud layer and the level of neutral buoyancy. Similarly, 38 "dried" profiles are produced by removing 1% from the RCE specific humidity at each level.

3. We run the RCE profile and each perturbed profile forward by a single time-step, with a strict enforcement of the weak temperature gradient approximation. In this framework, the residual heating in the free troposphere is exactly compensated by the large-scale vertical advection. The atmospheric radiation, convection, and radiation are fully interactive. The dry static energy and water vapor forcings are outputted to compute the four components of the linear response: convective moistening, convective heating, longwave heating and shortwave heating.

4. We select 10 linear responses to describe the response of RCE. Because of the extreme sensitivity of local entrainment to water vapor perturbations, the convection scheme often responds nonlinearly, in spite of the smallness of perturbations. For consistency, we

only select the linear responses, which produce the same response to within 20% of the Frobenius norm for the +1% and the -1% perturbations. Within the subset of linear responses (approximately half of the total set), we use the Metropolis Monte-Carlo algorithm (*Metropolis et al.* [1953], generalized by *Hastings* [1970]), in order to pick 10 time-steps from the RCE that minimize the residual heating rate at each level (i.e., that give the closest statistical fit to the RCE state).

5. We ensemble-average the 10 linear response matrices. Furthermore, we subtract the non-perturbed run from each perturbed run, in order to isolate the effect of the water vapor perturbation by removing the small drift present in each RCE snapshot.

6. We repeat steps 1-5 for four different fixed sea surface temperatures between 290K and 310K.

3. Results

In this section, we present the linear response matrix and its components. The matrices presented below are ensemble-average responses to a 1% moistening; as the response is linear for small perturbations, the matrices resulting from a 1% drying are nearly indistinguishable. In order to physically interpret these matrices, we have outputted the sub-components of the convective heating and moistening, following equations 27 and 29 of *Emanuel* [1991]. Since we are interpreting linear physics, the processes for the 1% drying case are the exact opposite of the processes for the 1% moistening case, presented below.

3.1. Radiative-convective equilibrium

The ensemble-average of RCE profiles is shown in Figure1: The specific humidity profile (Figure 1a) resembles typical tropical moisture profiles (e.g. Figure 2 of [*Beucler and Cronin*, 2016a] or [*Ciesielski et al.*, 2003]), with a surface value of 15.6g/kg and a column-integrated content of 35.7kg.m^{-2}. The temperature profile (Figure 1b) is moist-adiabatic in the lower and mid-troposphere (below 400hPa), with an average tropospheric lapse rate of 5.8K/km and a tropopause pressure of 100hPa. The stratosphere in the top 100hPa of the model includes strong shortwave heating associated with the prescribed ozone profile. The atmosphere is in radiative-convective equilibrium from the surface (1000hPa) to the level of neutral buoyancy (approximately 200hPa), as the convective heating and shortwave heating perfectly compensate the longwave cooling at each level. From the level of neutral buoyancy to the top of the model (0hPa), the atmosphere is in radiative equilibrium: the shortwave heating balances the longwave heating, and the convective heating is zero.

3.2. Convective response

The convective response (Figure 2) is defined as the sum of the convective moistening (M_{LH}) and the convective heating (M_{DSE}) responses (see Figure 3 for the decomposition). Water vapor perturbations at a given level are diffused to the two adjacent levels on a very short ($\sim$ 4hours) time-scale. Therefore, we average each growth rate on the diagonal with the two neighboring growth rates, to focus on non-numerical effects. The different zones of the matrix have different physics. Overall, the main effect of perturbing water vapor is to change the partial re-evaporation rate E (in s^{-1}) of cloudy water into the clear-sky environment. Moistening the environment decreases the humidity difference between the cloudy and clear-sky areas, and thus decreases the re-evaporation rate (in mathematical

terms: $\partial E/\partial q' < 0$) . According to the last equation of section 2.1, the water vapor growth rate associated to a change in re-evaporation is:

$$\frac{g}{L_v}\left(\underbrace{\frac{\partial^2 \mathcal{F}_{\mathrm{LH}}}{\partial p \partial q'}}_{\text{Moistening}} + \alpha \underbrace{\frac{\partial^2 \mathcal{F}_{\mathrm{DSE}}}{\partial p \partial q'}}_{\text{Latent heating}}\right)_{\mathrm{RCE}} = (1-\alpha)\left(\frac{\partial E}{\partial q'}\right)_{\mathrm{RCE}}. \tag{2}$$

According to equation 2, there are three possible situations:

1. $\alpha < 1$: The drying effect of decreasing re-evaporation overcomes the heating effect, leading to a damping of water vapor perturbations.

2. $\alpha = 1$: The drying effect of decreasing re-evaporation perfectly compensates the heating effect, consistent with zero change in the local moist static energy.

3. $\alpha > 1$: The heating effect of decreasing re-evaporation overcomes the drying effect, leading to an amplification of water vapor perturbations.

The leading physics of each zone is identified by breaking down the convective heating and moistening into its sub-components, following equations 27 and 29 of *Emanuel* [1991]:

(A) The local lower tropospheric response exhibits mildly positive growth rates, as $\alpha > 1$. The re-evaporation effect is partially compensated by a decrease in water vapor entrainment.

(B) We see strong positive growth rates for the local response at 600hPa, where HAM peaks above one. The re-evaporation effect adds to the moistening effect of the unsaturated downdrafts, which are locally attenuated by the moisture perturbation.

(C) In the upper troposphere, the local response is a damping of water vapor perturbations, as $\alpha < 1$. Another factor is the perturbation advection of water vapor by in-cloud updrafts, which dries the atmosphere more than it brings dry static energy in to moisten

it (since $\alpha < 1$).

(D) For this particular sounding, HAM peaks around 250hPa and exceeds 1, leading to a strongly positive growth rate.

(E) The effect of mid-tropospheric perturbations is to dry the lower-troposphere, through a combination of unsaturated downdraft amplification and an increase in the advection of moisture by in-cloud updrafts.

(F) The effect of upper tropospheric perturbations is to slightly moisten the lower troposphere through a small decrease in re-evaporation rate ($\alpha > 1$).

The general characteristics of the response are insensitive to the entrainment parameter (not shown): Although the value of the convective growth rates depends weakly on the entrainment parameter, the physics of the linear response of the Emanuel scheme are qualitatively unchanged.

3.3. Radiative response

The radiative response (Figure 4) is defined as the sum of the longwave cooling (M_{LW}) and the shortwave heating (M_{SW}) responses (see Figure 5 for the decomposition). The physics of this response can be separated in four parts, all dominated by the longwave effect:

(A) A strong local longwave cooling: Adding water vapor locally increases the emissivity of the atmospheric layer, making it cool to space faster.

(B) A significant indirect longwave heating effect: The levels below the moist perturbation emit less longwave radiation to space, resulting in a net heating. If integrated in the vertical, this remote longwave heating effect overcomes the local cooling effect, and the reader is referred to [*Beucler and Cronin*, 2016a] for more details on this positive

feedback.

(C) This indirect longwave heating effect is largest in the upper troposphere (above 330hPa). In this part of the atmosphere, the HAM has a large peak that exceeds 1, which proportionally increases the radiative growth rates. Furthermore, the RCE specific humidity is so small (smaller than 3g/kg) that even the most absorbing bands of the longwave spectrum are unsaturated. Small moist perturbations will thus increase the optical depth by a greater amount in these dry regions.

(D) The effect of radiative cooling is also amplified in the upper troposphere, including the levels above the moist perturbation, which receive less longwave radiation from the surface.

The shortwave heating acts in the opposite way, which attenuates all of the previous effects (A-D) by a typical factor of 1/3. The column-integrated growth rate is close to zero, except in the upper troposphere, where the remote longwave heating effect can lead to column-integrated growth rates over 1day^{-1}.

3.4. Full linear response

The total linear response matrix in the clear-sky case is obtained by summing each of its components. We summarize below the physics of its most important features:

(A) Lower tropospheric perturbations are locally damped through radiative cooling, which dominates over latent heating.

(B) Around 600hPa, the peak in HAM is strong enough for the convective heating to dominate over radiative cooling.

(C) Mid and upper tropospheric perturbations are locally damped through a combination of radiative cooling and convective drying.

(D) Radiative heating effects dominate over the drying effects of downdrafts, and mid to upper tropospheric perturbations moisten the mid-troposphere.

(E) Right below the tropopause, where HAM peaks, strong radiative and convective heating add up and lead to the largest growth rates .

From the appearance of the full linear response and the column-integrated growth rate, we can make several conclusions about the evolution of a small water vapor perturbation for short times. The upper-left part of the matrix is white and blue, corresponding to a damping of the water vapor field above the perturbation level. In contrast, most of the bottom-right part of the matrix is red, corresponding to an amplification of the water vapor field below the perturbation. As a consequence, we expect most perturbations to shift downwards in time, as a result of their interaction with clear-sky radiation and convection. Then, there are two zones where water vapor perturbations can potentially grow, with column-integrated growth rates of order $\widehat{M_{\text{uni}}} \approx 1\text{day}^{-1}$: lower tropospheric perturbations can grow locally through their interaction with convection, while upper tropospheric perturbations can lead to remote growth below the perturbation level, mostly through their interaction with radiation.

References

Arakawa, A., and W. H. Schubert (1974), Interaction of a Cumulus Cloud Ensemble with the Large-Scale Environment, Part I, doi:10.1175/1520-0469(1974)031⟨0674:IOACCE⟩2.0.CO;2.

Betts, A. K., and M. J. Miller (1986), A new convective adjustment scheme. Part II: Single column tests using GATE wave, BOMEX, ATEX and arctic air-mass data sets,

Quarterly Journal of the Royal Meteorological Society, *112*(473), 693–709, doi:10.1002/qj.49711247308.

Betts, A. K., and M. J. Miller (1993), *The Betts-Miller Scheme*, pp. 107–121, American Meteorological Society, Boston, MA, doi:10.1007/978-1-935704-13-3_9.

Beucler, T., and T. W. Cronin (2016a), Moisture-radiative cooling instability, doi:10.1002/2016MS000763.

Beucler, T., and T. W. Cronin (2016b), Moisture-radiative cooling instability, doi:10.1002/2016MS000763.

Bjerknes (1938), Saturated-adiabatic ascent of air, (2), 325–330.

Bolton, D. (1980), The Computation of Equivalent Potential Temperature, *Monthly Weather Review*, *108*(7), 1046–1053, doi:10.1175/1520-0493(1980)108⟨1046:TCOEPT⟩2.0.CO;2.

Bony, S., B. Stevens, D. Coppin, T. Becker, K. A. Reed, A. Voigt, and B. Medeiros (2016), Thermodynamic control of anvil cloud amount, *Proceedings of the National Academy of Sciences*, *113*(32), 8927–8932, doi:10.1073/pnas.1601472113.

Bretherton, C. S., P. N. Blossey, and M. Khairoutdinov (2005), An Energy-Balance Analysis of Deep Convective Self-Aggregation above Uniform SST, *Journal of the Atmospheric Sciences*, *62*(12), 4273–4292, doi:10.1175/JAS3614.1.

Chikira, M. (2014), Eastward-Propagating Intraseasonal Oscillation Represented by Chikira Sugiyama Cumulus Parameterization. Part II: Understanding Moisture Variation under Weak Temperature Gradient Balance, *Journal of the Atmospheric Sciences*, *71*(2), 615–639, doi:10.1175/JAS-D-13-038.1.

Ciesielski, P. E., R. H. Johnson, P. T. Haertel, and J. Wang (2003), Corrected TOGA COARE sounding humidity data: Impact on diagnosed properties of convection and climate over the warm pool, *Journal of Climate*, *16*(14), 2370–2384, doi:10.1175/2790.1.

Coppin, D., and S. Bony (2017), Internal variability in a coupled General Circulation Model in Radiative-Convective Equilibrium, *Geophysical Research Letters*, doi:10.1002/2017GL073658.

Dee, D. P., S. M. Uppala, A. J. Simmons, P. Berrisford, P. Poli, S. Kobayashi, U. Andrae, M. A. Balmaseda, G. Balsamo, P. Bauer, P. Bechtold, A. C. M. Beljaars, L. van de Berg, J. Bidlot, N. Bormann, C. Delsol, R. Dragani, M. Fuentes, A. J. Geer, L. Haimberger, S. B. Healy, H. Hersbach, E. V. Holm, L. Isaksen, P. Kollberg, M. Kohler, M. Matricardi, A. P. Mcnally, B. M. Monge-Sanz, J. J. Morcrette, B. K. Park, C. Peubey, P. de Rosnay, C. Tavolato, J. N. Thopaut, and F. Vitart (2011), The ERA-Interim reanalysis: Configuration and performance of the data assimilation system, *Quarterly Journal of the Royal Meteorological Society*, *137*(656), 553–597, doi:10.1002/qj.828.

Emanuel, K. a. (1991), A Scheme for Representing Cumulus Convection in Large-Scale Models, doi:10.1175/1520-0469(1991)048⟨2313:ASFRCC⟩2.0.CO;2.

Emanuel, K. A. (1994), *Atmospheric convection*, 1–580 pp., Oxford University Press.

Emanuel, K. A., and M. Živković-Rothman (1999), Development and Evaluation of a Convection Scheme for Use in Climate Models, *Journal of the Atmospheric Sciences*, *56*(11), 1766–1782, doi:10.1175/1520-0469(1999)056⟨1766:DAEOAC⟩2.0.CO;2.

Emanuel, K. a., A. a. Wing, and E. M. Vincent (2014), Radiative-convective instability, *Journal of Advances in Modeling Earth Systems*, *5*(November), n/a–n/a, doi:10.1002/2013MS000270.

Fouquart, Y., and B. Bonnel (1980), Computations of solar heating of the earth's atmosphere- A new parameterization, *Beitraege zur Physik der Atmosphaere*, *53*, 35–62.

Frierson, D. M. W. (2007), The Dynamics of Idealized Convection Schemes and Their Effect on the Zonally Averaged Tropical Circulation, *Journal of the Atmospheric Sciences*, *64*(6), 1959–1976, doi:10.1175/JAS3935.1.

Grabowski, W. W., and M. W. Moncrieff (2004), Moisture-convection feedback in the tropics, *Quarterly Journal of the Royal Meteorological Society*, *130*(604), 3081–3104, doi:10.1256/qj.03.135.

Hannah, W. M., and E. D. Maloney (2011), The role of moisture-convection feedbacks in simulating the Madden-Julian oscillation, *Journal of Climate*, *24*(11), 2754–2770, doi:10.1175/2011JCLI3803.1.

Hartman, P. (1960), A lemma in the theory of structural stability of differential equations, *Proceedings of the American Mathematical Society*, *11*(4), 610–610, doi: 10.1090/S0002-9939-1960-0121542-7.

Hartmann, D. L., and K. Larson (2002), An important constraint on tropical cloud - climate feedback, *Geophysical Research Letters*, *29*(20), 12–1–12–4, doi:10.1029/2002GL015835.

Hastings, W. K. (1970), Monte carlo sampling methods using Markov chains and their applications, *Biometrika*, *57*(1), 97–109, doi:10.1093/biomet/57.1.97.

Herman, M. J., and Z. Kuang (2013), Linear response functions of two convective parameterization schemes, *Journal of Advances in Modeling Earth Systems*, *5*(3), 510–541, doi:10.1002/jame.20037.

Holloway, C. E., and J. D. Neelin (2009), Moisture Vertical Structure, Column Water Vapor, and Tropical Deep Convection, *Journal of the Atmospheric Sciences*, *66*(6), 1665–1683, doi:10.1175/2008JAS2806.1.

Holloway, C. E., and S. J. Woolnough (2016), The sensitivity of convective aggregation to diabatic processes in idealized radiative-convective equilibrium simulations, *Journal of Advances in Modeling Earth Systems*, *8*(1), 166–195, doi:10.1002/2015MS000511.

Iacono, M. J., E. J. Mlawer, S. A. Clough, and J.-J. Morcrette (2000), Impact of an improved longwave radiation model, RRTM, on the energy budget and thermodynamic properties of the NCAR community climate model, CCM3, *Journal of Geophysical Research: Atmospheres*, *105*(D11), 14,873–14,890, doi:10.1029/2000JD900091.

Iacono, M. J., J. S. Delamere, E. J. Mlawer, M. W. Shephard, S. A. Clough, and W. D. Collins (2008), Radiative forcing by long-lived greenhouse gases: Calculations with the AER radia- tive transfer models, *Journal of Geophysical Research Atmospheres*, *113*(D13103), doi:10.1029/2008jd009944.

Inoue, K., and L. Back (2015), Column-Integrated Moist Static Energy Budget Analysis on Various Time Scales during TOGA COARE, *Journal of the Atmospheric Sciences*, *72*(5), 1856–1871, doi:10.1175/JAS-D-14-0249.1.

Kuang, Z. (2010), Linear Response Functions of a Cumulus Ensemble to Temperature and Moisture Perturbations and Implications for the Dynamics of Convectively Coupled Waves, *Journal of the Atmospheric Sciences*, *67*(4), 941–962, doi:10.1175/2009JAS3260.1.

Kuang, Z. (2012), Weakly Forced Mock Walker Cells, *Journal of the Atmospheric Sciences*, *69*(9), 2759–2786, doi:10.1175/JAS-D-11-0307.1.

Malkus, J. S., C. Ronne, and M. Chafee (1961), Cloud Patterns in Hurricane Daisy, 1958, *Tellus*, *13*(1), 8–30, doi:10.1111/j.2153-3490.1961.tb00062.x.

Mapes, B., and R. Neale (2011), Parameterizing convective organization to escape the entrainment dilemma, *Journal of Advances in Modeling Earth Systems*, *3*(2), n/a–n/a, doi:10.1029/2011MS000042.

Metropolis, N., A. W. Rosenbluth, M. N. Rosenbluth, A. H. Teller, and E. Teller (1953), Equation of State by Fast Computing Machines, *The Journal of Chemical Physics*, *21*(1953), 1087–1092, doi:10.1063/1.1699114.

Mlawer, E. J., S. J. Taubman, P. D. Brown, M. J. Iacono, and S. A. Clough (1997), Radiative transfer for inhomogeneous atmospheres: RRTM, a validated correlated-k model for the longwave, *Journal of Geophysical Research: Atmospheres*, *102*(D14), 16,663–16,682, doi:10.1029/97JD00237.

Morcrette, J.-J. (1991), Radiation and cloud radiative properties in the European Centre for Medium Range Weather Forecasts forecasting system, *Journal of Geophysical Research*, *96*(D5), 9121, doi:10.1029/89JD01597.

Muller, C., and S. Bony (2015), What favors convective aggregation and why ?, pp. 5626–5634, doi:10.1002/2015GL064260.Received.

Muller, C. J., and I. M. Held (2012), Detailed Investigation of the Self-Aggregation of Convection in Cloud-Resolving Simulations, *Journal of the Atmospheric Sciences*, *69*, 2551–2565, doi:10.1175/JAS-D-11-0257.1.

Pauluis, O. M., and A. A. Mrowiec (2013), Isentropic Analysis of Convective Motions, *Journal of the Atmospheric Sciences*, *70*(11), 3673–3688, doi:10.1175/JAS-D-12-0205.1.

Pierrehumbert, R. T. (2009), Principles of Planetary Climate, *Earth*, *1*, 359.

Plant, R. S. (2009), A review of the theoretical basis for bulk mass flux convective parameterization, *Atmospheric Chemistry and Physics*, pp. 3529–3544, doi:10.5194/acpd-9-24945-2009.

Ramanathan, V., and J. A. Coakley (1978), Climate modeling through radiative-convective models, *Reviews of Geophysics*, *16*(4), 465–489, doi:10.1029/RG016i004p00465.

Renno, N. O., P. H. Stone, and K. A. Emanuel (1994), Radiative-convective model with an explicit hydrologic cycle. 2: Sensitivity to large changes in solar forcing, doi:10.1029/94JD01332.

Romps, D. M. (2014), An analytical model for tropical relative humidity, *Journal of Climate*, *27*(19), 7432–7449, doi:10.1175/JCLI-D-14-00255.1.

Sengupta, D., B. N. Goswami, and R. Senan (2001), Coherent intraseasonal oscillations of ocean and atmosphere during the Asian summer monsoon, *Geophysical Research Letters*, *28*(21), 4127–4130, doi:10.1029/2001GL013587.

Sherwood, S. C., W. Ingram, Y. Tsushima, M. Satoh, M. Roberts, P. L. Vidale, and P. A. O'Gorman (2010), Relative humidity changes in a warmer climate, *Journal of Geophysical Research Atmospheres*, *115*(9), D09,104, doi:10.1029/2009JD012585.

Singh, M. S., and P. A. O'Gorman (2013), Influence of entrainment on the thermal stratification in simulations of radiative-convective equilibrium, *Geophysical Research Letters*, *40*(16), 4398–4403, doi:10.1002/grl.50796.

Sobel, A. H., J. Nilsson, and L. M. Polvani (2001), The Weak Temperature Gradient Approximation and Balanced Tropical Moisture Waves*, *Journal of the Atmospheric Sciences*, *58*, 3650–3665, doi:10.1175/1520-0469(2001)058⟨3650:TWTGAA⟩2.0.CO;2.

Tompkins, A. M. (2001), Organization of Tropical Convection in Low Vertical Wind Shears: The Role of Cold Pools, *Journal of the Atmospheric Sciences*, *58*, 1650–1672, doi:10.1175/1520-0469(2001)058⟨1650:OOTCIL⟩2.0.CO;2.

Vecchi, G. A., and D. E. Harrison (2002), Monsoon breaks and subseasonal sea surface temperature variability in the Bay of Bengal, *Journal of Climate*, *15*(12), 1485–1493, doi:10.1175/1520-0442(2002)015⟨1485:MBASSS⟩2.0.CO;2.

Wing, A. A., and T. W. Cronin (2016), Self-aggregation of convection in long channel geometry, *Quarterly Journal of the Royal Meteorological Society*, *142*(694), 1–15, doi: 10.1002/qj.2628.

Wing, A. a., and K. a. Emanuel (2014), Physical mechanisms controlling self-aggregation of convection in idealized numerical modeling simulations, *Journal of Advances in Modeling Earth Systems*, *5*(November), 59–74, doi:10.1002/2013MS000269.

Wing, A. A., S. J. Camargo, and A. H. Sobel (2016), Role of radiative-convective feedbacks in spontaneous tropical cyclogenesis in idealized numerical simulations, *Journal of the Atmospheric Sciences*, *73*(7), JAS–D–15–0380.1, doi:10.1175/JAS-D-15-0380.1.

Wing, A. A., K. Emanuel, C. E. Holloway, and C. Muller (2017), Convective Self-Aggregation in Numerical Simulations: A Review, *Surveys in Geophysics*, doi:10.1007/s10712-017-9408-4.

Wolding, B. O., E. D. Maloney, S. Henderson, and M. Branson (2017), Climate Change and the Madden-Julian Oscillation : A Vertically Resolved Weak Temperature Gradient Analysis, *Journal of Advances in Modeling Earth Systems*, doi:10.1002/2016MS000843.

Yanai, M., S. Esbensen, and J.-H. Chu (1973), Determination of Bulk Properties of Tropical Cloud Clusters from Large-Scale Heat and Moisture Budgets, doi:10.1175/

1520-0469(1973)030⟨0611:DOBPOT⟩2.0.CO;2.

Yu, J.-Y., C. Chou, and J. D. Neelin (1998), Estimating the Gross Moist Stability of the Tropical Atmosphere*, *Journal of the Atmospheric Sciences*, *55*(8), 1354–1372, doi: 10.1175/1520-0469(1998)055⟨1354:ETGMSO⟩2.0.CO;2.

Parameter	Value	Units
Auto-conversion threshold	1.1	mg/g
Convective momentum transport coefficient	0.7	
Critical temperature for precipitation	−55.0	°C
Entrainment parameter	1.5	
Evaporation coefficient of rain	0.9	
Evaporation coefficient of snow	0.6	
Fraction of precipitation falling outside the clouds	0.12	
Fractional area of unsaturated downdrafts	0.05	
Gust factor for surface fluxes	5.0	$m.s^{-1}$
Length of integration for RCE runs	400.0	day
Pressure fall speed of rain	50.0	$Pa.s^{-1}$
Pressure fall speed of snow	5.0	$Pa.s^{-1}$
Quasi-equilibrium relaxation coefficient α_{QE}	0.015	$kg.m^{-2}.s^{-1}.K^{-1}$
Quasi-equilibrium relaxation coefficient DAMP	0.05	
Solar constant	1360	$W.m^{-2}$
Surface albedo	0.10	
Timestep	180	s

Table 1. Parameters used in the MIT single-column model

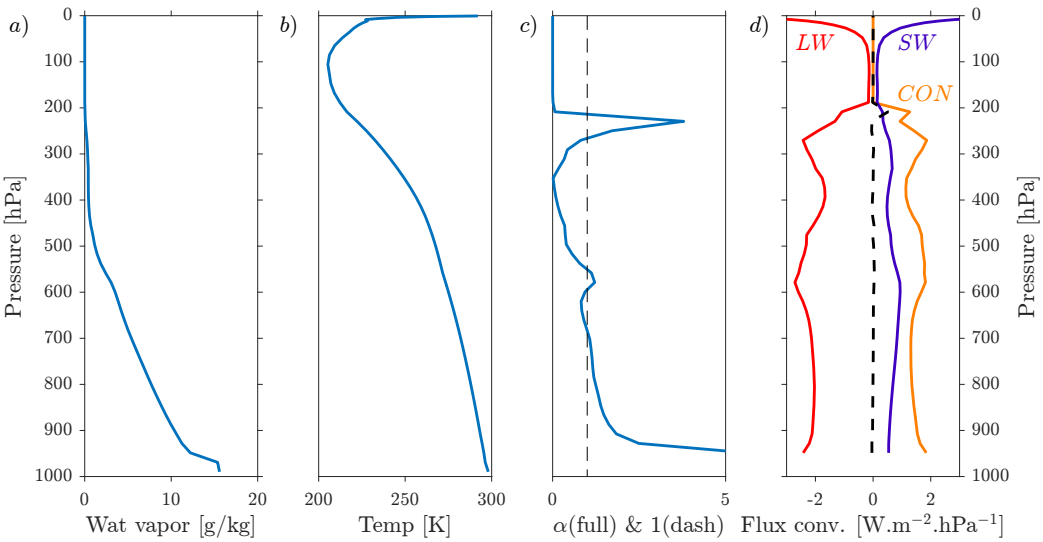

Figure 1. (a) Specific humidity (in g/kg), (b) HAM (c) temperature (in K) and (d) flux convergence (in W.m^{-2}.hPa^{-1}) profiles. In panel (d), the longwave radiative heating is red, the shortwave radiative heating blue, the convective heating orange, and the total convergence flux is represented by ad dotted black line. The profiles are ensemble averages of the 10-members chosen to represent radiative-convective equilibrium. The surface temperature is fixed to 300K and cloud-radiation interactions are deactivated.

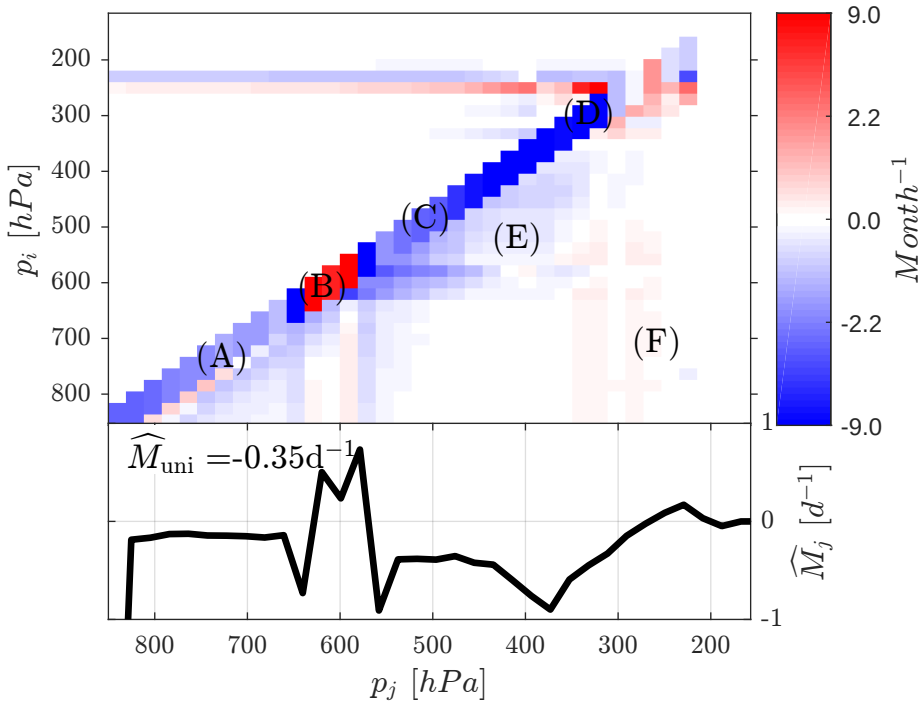

Figure 2. (Top) Convective component of the linear response matrix ($M_{\text{LH}} + M_{\text{DSE}}$), in units month^{-1}.

(Bottom) Vertically-integrated growth rates (in units day^{-1}) versus perturbation level (in hPa).

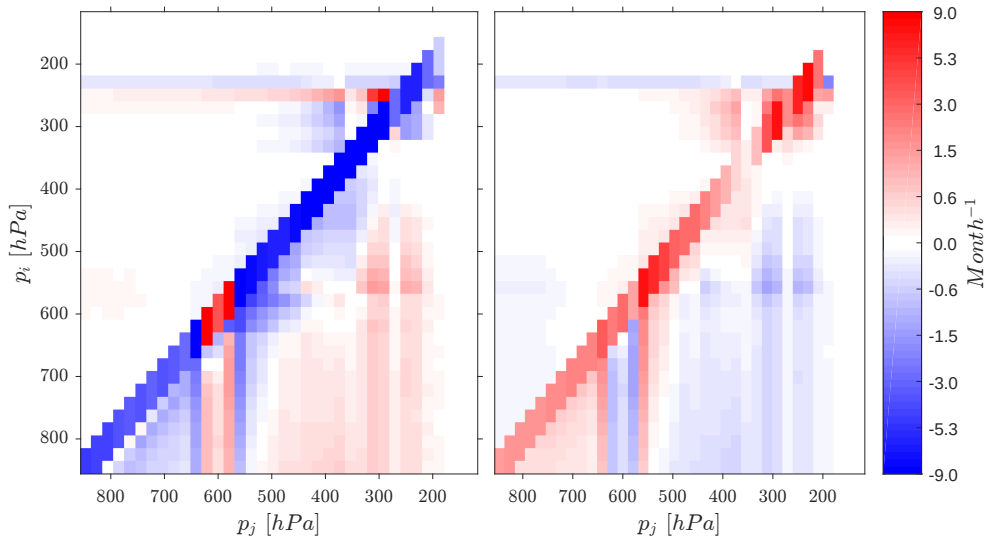

Figure 3. (a) Convective moistening (M_{LH}) and (b) Convective heating (M_{DSE}) linear response matrices, in units month^{-1}.

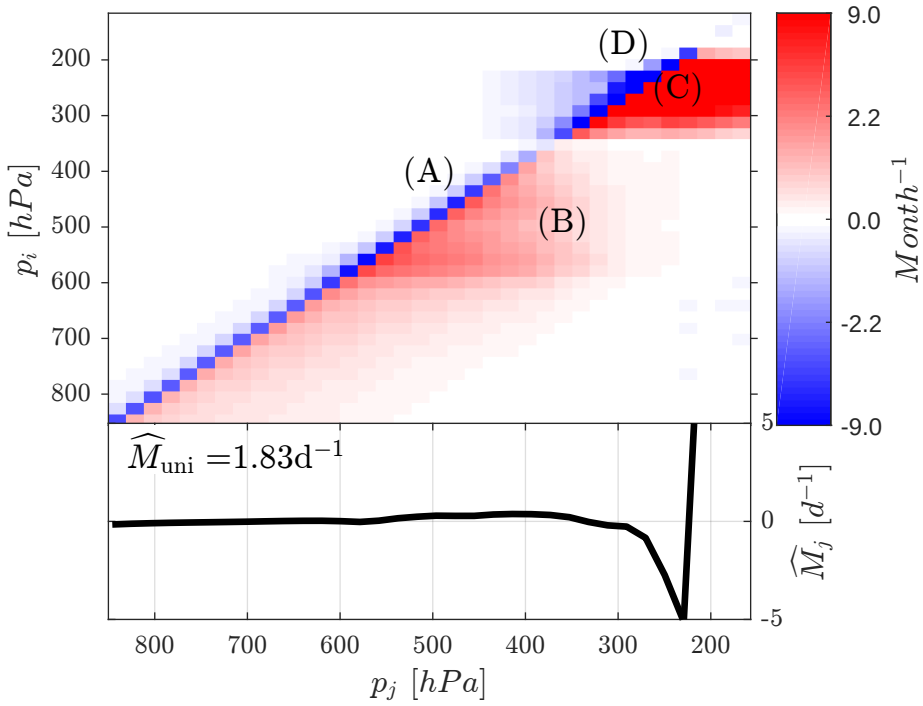

Figure 4. (Top) Radiative component of the linear response matrix ($M_{\text{LW}} + M_{\text{SW}}$), in units month^{-1}.

(Bottom) Column-integrated growth rates (in units day^{-1}) versus perturbation level (in hPa). Letters indicate effects that are described in the text.

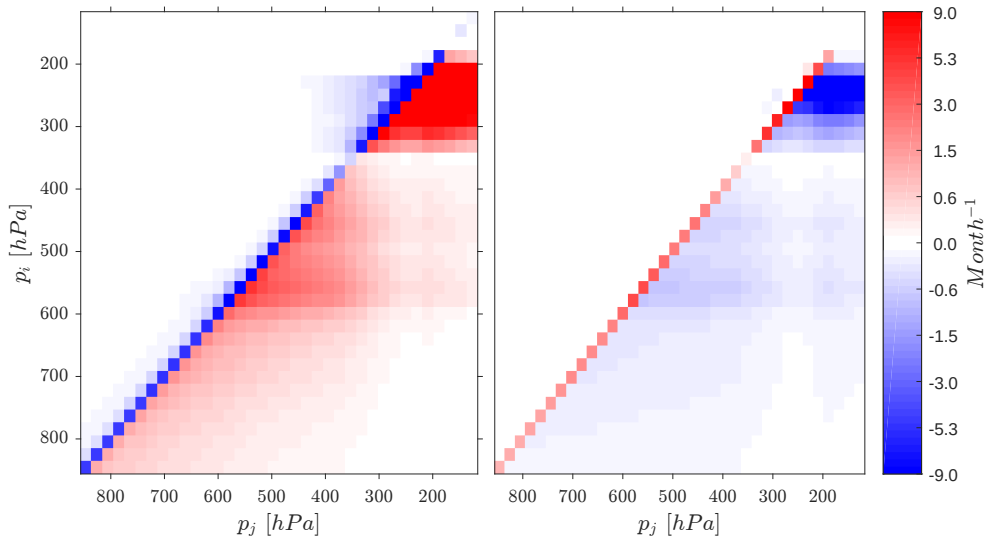

Figure 5. (a) Longwave (M_{LW}) and (b) Shortwave (M_{SW}) linear response functions, in units month^{-1}.

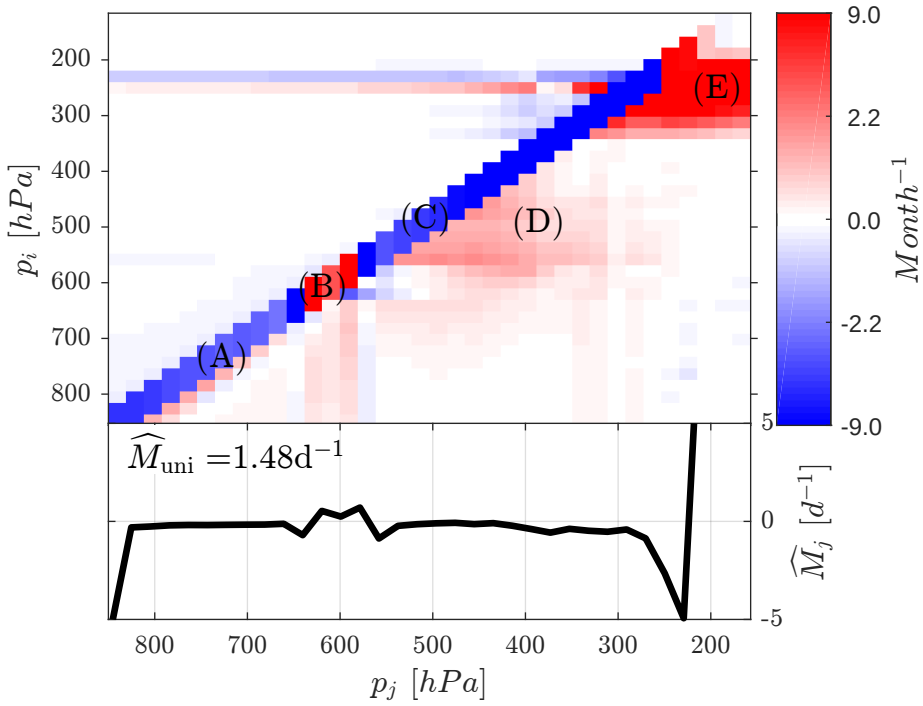

Figure 6. (Top) Full linear response matrix (M), in units month^{-1}. (Bottom) Column-integrated growth rates (in units day^{-1}) versus perturbation level (in hPa).